Desalination and Water Treatment
www.deswater.com

doi: 10.5004/dwt.2023.30083

313 (2023) 12–25
November

Modeling of heat and mass transfer in vacuum membrane distillation for seawater desalination

Zakaria Triki[a,*], Zineb Fergani[a], Hichem Tahraoui[a,b]

[a]*Laboratory of Biomaterials and Transport Phenomena, University of Medea, Medea 26000, Algeria, email: triki.zakaria@univ-medea.dz (Z. Triki)*
[b]*Laboratory of Chemical Process Engineering, University of Ferhat Abbas, Setif 19000, Algeria*

Received 7 July 2023; Accepted 3 October 2023

ABSTRACT

Vacuum membrane distillation (VMD) is an attractive method for water desalination due to its high pure water permeability under lower operating temperatures, resulting in less energy consumption, lower heat loss via conduction through the membrane surface, and negligible heat transfer by conduction due to the low pressure on the permeate side. The aim of this study is to establish a comprehensive numerical model that describes the water vapor transfer across a hydrophobic micro-porous membrane in single-stage and multi-stage VMD processes for seawater desalination. The numerical predictions are compared to previous experimental data, and a good correlation is observed. The investigation also conducted a sensitivity analysis of process variables and membrane specifications on VMD performance, as well as an assessment of the impact of temperature and concentration polarization. The obtained results showed that the permeation flux reached 18.42 kg/m^2·h at 35 g/L feed concentration, 65°C feed temperature, 50 L/h feed flow rate, and 3 kPa vacuum pressure. Moreover, the findings revealed that feed temperature was the most significant factor, while feed flow rate was the least important in determining permeation flux. Additionally, the results indicated that the structure and porosity of support materials play important roles in determining the performance of VMD process. Finally, results confirmed that temperature polarization had a more significant effect on the reduction of permeate flux than concentration polarization.

Keywords: Seawater desalination; Vacuum membrane distillation; Heat and mass transfer; Modeling; Performance

1. Introduction

The potential of vacuum membrane distillation (VMD) is gaining increasing interest due to its effectiveness in diverse applications, such as separating aqueous solutions and eliminating gases and volatile organic compounds from water [1–3]. VMD presents numerous benefits in seawater desalination [4,5], and it is not greatly affected by temperature polarization occurring at the membrane surface. In addition, heat conduction losses through the membrane are significantly decreased, and in certain instances, they are insignificant [6]. Nonetheless, the principal disadvantage of VMD pertains to the intricate configuration involving vacuum and external condensers [7,8], as well as the potential for the applied vacuum to produce substantial pressure fluctuations on the membrane surface, which may result in wetting or reduced hydrophobicity of the membrane. These factors can negatively impact the quality of the permeate produced [9,10].

To ensure the successful and reliable application of MD technology, it is essential to gain a comprehensive understanding of the processes occurring in the MD membrane and module through mathematical modeling [11–13]. The primary aim of MD modeling is to forecast the permeate

* Corresponding author.

flux and how it relates to the MD module configuration, membrane properties, and operational parameters [14–16]. Various mathematical models for MD have been created and documented in literature, with most studies concentrating on direct contact MD (DCMD) modeling due to its simplicity, while other MD configurations have been given less attention [17,18]. There is still active development in the analysis and modeling of MD, with efforts being made to promote the efficient use of VMD in desalination [4,19].

Various experimental investigations have been conducted, and models have been developed to identify the key factors that could influence VMD membrane modules, permeation flux, and energy consumption. The performance sensitivity of a particular membrane typically corresponds to factors such as the temperature of the feedwater, the applied vacuum pressure, and the concentration of solutes in the feed solution. To predict the permeation flux across MD membranes, the dusty-gas model (DGM), which is commonly utilized for characterizing mass transfer in porous materials is employed [20,21].

Soni et al. [22] established a mathematical model that accounts for the temperature-dependent physical properties of the fluid to describe the transport mechanisms in VMD. Both experimental and modeling outcomes indicate that the permeate flux rises with a reduction in the vacuum pressure (higher vacuum) and an increase in the flow rate of the feed fluid. A study by Banat et al. [1] conducted a sensitivity analysis of the operational conditions and revealed that the mass transfer across the membrane is highly responsive to the feed temperature, especially in the case of higher vacuum, whereas it is more sensitive to the vacuum pressure when low feed temperatures are employed.

Similarly, Upadhyaya et al. [23] carried out a sensitivity investigation of the desalination process through VMD and observed that the mass flow is significantly influenced by factors such as thickness, tortuosity, porosity, and pore diameter of the membrane, while remaining sensitive to the vacuum pressure and feed temperature. Mericq et al. [4] also emphasized the significance of membrane permeability and demonstrated the potential for VMD to compete with reverse osmosis (RO) in terms of energy efficiency, provided that a suitable membrane is selected.

Lee and Kim [24] employed a one-dimensional VMD method in their research to predict the efficiency of seawater desalination by evaluating the effectiveness of VMD modules of the hollow fiber type. The study evaluated specific energy consumption and productivity and scrutinized the primary operating parameters that influence VMD performance under varying conditions, such as temperature, velocity, and mass fraction, as well as the effects of module dimensions, including module length and the number of fibers. Wang et al. [25] created a two-dimensional model using the finite element method in hollow fibers for VMD and discovered that optimal conditions can lead to a cost reduction of up to 38% in water production.

Hayer et al. [26] created a numerical model based on the principles of fluid mechanics and heat and mass transfer to analyze various parameters affecting VMD in hollow fiber membrane modules. The study found that increased feed flow and temperature resulted in higher transmembrane flux, but the effect of feed flow rate on VMD separation performance decreased at certain rates. The model also identified the main mechanisms involved in the diffusion process inside the membrane module, with diffusion being the most significant factor, followed by viscous flow. Additionally, the model estimated the individual contributions of Knudsen diffusion, free diffusion, and viscous flow.

Kim et al. [27] presented an extensive mathematical model of the hollow-fiber VMD process for seawater desalination. This model incorporated mass, momentum, and energy balances, as well as the transmembrane flux model. The researchers discovered that a basic VMD model could potentially overestimate the mean permeate flux, as the detailed model accounted for pressure build-up in the fiber lumen. Liu et al. [28] employed numerical simulations to investigate hollow fiber VMD by taking into account mass, energy, and momentum transfer and treating the membrane as a functional surface. Nevertheless, the study did not incorporate the impact of concentration on the vapor pressure in the boundary condition equations of the membrane.

Asghari et al. [29] integrated both mass and heat transfer models into a VMD system and validated the models with experimental data. The impact of several operating parameters such as feed temperature, vacuum pressure on the permeate side, feed concentration, and heat transfer coefficient on the permeate flux was also investigated. According to their results, increasing feed temperature and heat transfer coefficient enhanced the permeate flux, while increasing vacuum pressure and feed concentration caused a decrease in the permeate flux.

The use of artificial neural networks (ANNs) for simulating mass transfer in VMD was explored by Dragoi and Vasseghian [30], with the aim of predicting the permeate flux for the treatment of radioactive wastewater. The study compared various ANN structures to identify the optimal model for the system and optimized the VMD process to determine the most favorable operating conditions that would maximize the mass transfer rate.

Ibrahim and Alsalhy [31] developed a mathematical model that accounts for both heat and mass transfer during VMD to examine how changes in membrane properties during the process affect permeation flux. The model divided the module into several cells and solved a system of nonlinear equations numerically. The researchers also explored the impact of module properties, operating conditions, and membrane characteristics on water permeation flux.

Previous modeling studies on VMD have mainly focused on predicting permeate flux and its dependence on various factors. There is a lack of research on the impact of concentration polarization on membrane scaling and how MD modeling can reduce this issue through appropriate module, membrane, and parameter optimization. Additionally, the influence of stirring rates on the feed and permeate sides of MD modules on transmembrane flux has not been thoroughly explored. Consequently, further studies using MD modeling are required to consider the impact of stirring rate and the interplay between MD operational parameters on permeate flux in current configurations [15].

Recently, multi-stage vacuum membrane distillation (M-VMD) desalination systems have gained more attention as means of enhancing the performance of single-stage configuration. In the literature, various modeling approaches

have been used to predict the performance of M-VMD systems under different operating conditions, such as feed flow rate, temperature, and pressure. Some studies have proposed mathematical models which have been validated using experimental data. Other studies have used computational fluid dynamics (CFD) to model the flow behavior and heat transfer in M-VMD systems, providing insights into the design and optimization of these systems.

Empirical models have also been developed to predict the performance of M-VMD systems based on experimental data [32–36]. One of the challenges in modeling M-VMD systems is accounting for the effects of concentration polarization and scaling, which can significantly affect the performance of the system. Furthermore, the effects of stirring rates on the feed and permeate sides of MD modules on transmembrane flux have not been extensively investigated.

This study aims to develop a comprehensive model that can accurately represent the water vapor transfer process through a hydrophobic micro-porous membrane in single-stage and multi-stage VMD systems for seawater desalination. The model is developed to consider temperature and concentration polarization effects. A sensitivity analysis is also performed to examine how various operational conditions, including feed water temperature, feed flow rate, feed concentration, and vacuum pressure, can influence the performance of the VMD system.

2. VMD modeling

2.1. Single-stage VMD

VMD uses a membrane as a selective barrier to permit vapor to pass through, while preventing liquid and impurities from crossing. The vapor that permeates through the membrane is condensed and collected as permeate. The difference in vapor pressure between the feed and permeate sides of the membrane drives the process, and applying a vacuum to the permeate side increases this pressure difference, resulting in better separation efficiency. The process of VMD takes place in a tangential flow cell where a hollow-fiber membrane is used for the simultaneous transfer of heat and mass, as shown in Fig. 1. Heat transfer happens in the liquid, solid, and gas phases, while mass transfer happens only in the liquid and gas phases [37].

The Knudsen flow model is used in the study for the numerical simulation of heat and mass transfer since it covers most of the mass transport mechanisms in the VMD process [22]. The model is simplified using the following assumptions:

- A steady-state process is assumed.
- Momentum transfer within the vacuum domain is negligible.
- Heat transfer in the permeate domain and conductive heat transfer through the membrane are negligible.
- Mass transfer within the permeate is neglected and the mass fraction of water vapor is assumed to be unity.
- The distillate is salt-free.

When water is mass transported through the membrane, the water vapor flux, J_w is expressed [38,39]:

$$J_w = B_m\left(P_m\left(T_m, C_m\right) - P_v\right) \tag{1}$$

where B_m is the VMD coefficient of the membrane, T_m is the membrane surface feed temperature, C_m is the solute concentration on the membrane surface in the feed side, $P_m(T_m, C_m)$ is the water vapor pressure on the membrane surface in the feed side, and P_v is the pressure in the vacuum side.

In the Knudsen flow model the membrane coefficient, B_m is expressed [40]:

$$B_m = \frac{MD^{\mathrm{kn}}}{RT_m\delta} \tag{2}$$

D^{kn} is the diffusion coefficient of solute given by:

$$D^{\mathrm{kn}} = \frac{2\varepsilon r}{3\tau}\left(\frac{8RT_m}{\pi M}\right)^{0.5} \tag{3}$$

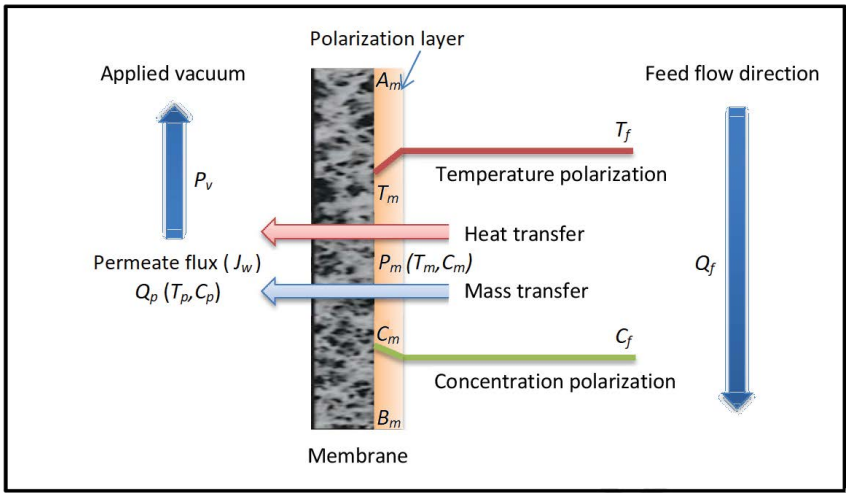

Fig. 1. Schematic of heat and mass transfer in VMD process.

where ε is porosity, r is the pore radius, r is the membrane thickness, τ is the pore tortuosity, M is the molecular mass of water, and R is the gas constant.

Table 1 presents the key properties of the membranes used in the study [41].

The membrane surface vapor pressure, $P_m(T_m,C_m)$ is expressed using Raoult's law which is valid over a very wide range of temperatures and concentrations ($0 < T < 200$°C and $0 < S < 240$ g/kg) [42]:

$$P_m\left(T_m,C_m\right)=\frac{\exp\begin{bmatrix}\left(-5.80\times10^{3}/T_m\right)+1.39\\-4.86\times10^{-2}T_m+4.18\times10^{-5}T_m^{2}\\+\left(-1.45\times10^{-8}T_m^{3}\right)+6.55\log T_m\end{bmatrix}}{1+0.57257\left(C_m/\left(1000-C_m\right)\right)} \tag{4}$$

MD systems employ both latent and conductive heat transfer to transport heat. In the presence of a boundary layer on the membrane surface, the temperature at that surface is lower than the feed temperature. However, due to the low pressure on the permeate side, VMD systems experience minimal conductive heat transfer across the membrane. As a result, the heat flux through the liquid boundary layer can be described by Eq. (5) [43]:

$$h_w\left(T_f-T_m\right)=J_w\Delta H_v \tag{5}$$

where ΔH_v is the latent heat of vaporization, h_w is the heat transfer coefficient, and T_f is the feed temperature.

The heat transfer coefficient, h_w is calculated [22,44]:

$$h_w=\frac{\lambda_w\cdot\mathrm{Nu}}{d_h} \tag{6}$$

with

$$\mathrm{Nu}=1.86\left(\mathrm{Re}\times\mathrm{Pr}\times\frac{d_h}{L}\right)^{0.33}\quad \mathrm{Re}<2100:\text{Laminar flow} \tag{7}$$

or

$$\mathrm{Nu}=0.023\,\mathrm{Re}^{0.8}\,\mathrm{Pr}^{0.33}\quad \mathrm{Re}>4000:\text{Turbulent flow} \tag{8}$$

where λ_w is the thermal conductivity of the water, d_h is the hydraulic diameter and L is the length of the channel.

Nu, Re and Pr are the Nusselt, Reynolds and Prandtl numbers, respectively.

$$\mathrm{Re}=\frac{\rho_w\cdot v\cdot d_h}{\mu_w} \tag{9}$$

$$\mathrm{Pr}=\frac{C_{p,w}\cdot\mu}{\lambda_w} \tag{10}$$

where ρ is the water density, $C_{p,w}$ is the water heat capacity, μ is the water dynamic viscosity, and μ is the feed flow velocity.

Thermophysical properties of seawater are taken from the correlations provided by Sharqawy et al. [42] as a function of temperature and salinity.

Assuming steady-state operation, the mass balance equation for the feed solution can be written as:

$$Q_fC_f=Q_pC_p \tag{11}$$

where Q_f is the volumetric flow rate of the feed solution, C_f is the concentration of the feed solution, Q_p is the volumetric flow rate of the permeate, and C_p is the concentration of the permeate.

The permeate flux, J_w is defined as the volume of permeate produced per unit area of the membrane per unit time, and is given by:

$$J_w=\frac{Q_p}{A_m} \tag{12}$$

where A_m is the membrane area.

By combining the above equations, the feed flow rate can be expressed as:

$$Q_f=\frac{J_w\cdot A_m}{C_f} \tag{13}$$

The temperature polarization coefficient (TPC) is a measure of the polarization effect that results from differences in temperature. It is usually defined as the ratio of the actual driving force to the theoretical driving force and can be represented by Eq. (14) [39,45]:

$$\mathrm{TPC}=\frac{T_w-T_p}{T_f-T_p} \tag{14}$$

where T_p is the permeate side temperature.

The concentration profile of salt on the membrane surface can be determined using the equation below [46,47], which employs film theory to account for concentration polarization:

$$\frac{C_m}{C_f}=\exp\left(\frac{J_w}{k}\right) \tag{15}$$

Table 1
Properties of the membrane module [41]

Membrane type	Polypropylene (PP)
Thickness (μm)	210
Porosity (%)	50–70
Tortuosity (–)	1.4
Average pore size (μm)	0.3–0.7
Effective length of fiber (mm)	100–250
Effective membrane area (mm²)	28×10^{2}
Average speed of vapor molecular (m/s)	20
Long of cross-section of the flow channel (mm)	3.4
Length of cross-section of the flow channel (mm)	3.3

The mass transfer coefficient, k, can be calculated by the relationship of the dimensionless number [48,49]:

$$k = \frac{\mathrm{Sh} \times D^{\mathrm{kn}}}{d_h} \tag{16}$$

With:

$$\mathrm{Sh} = 1.86\left(\mathrm{Re} \times \mathrm{Sc} \times \frac{d_h}{L}\right)^{0.33} \quad \mathrm{Re} < 2100 : \text{Laminar flow} \tag{17}$$

or

$$\mathrm{Sh} = 0.023\,\mathrm{Re}^{0.8}\,\mathrm{Sc}^{0.33} \quad \mathrm{Re} > 4000 : \text{Turbulent flow} \tag{18}$$

where Sh is Sherwood number and Sc is Schmidt number.

Schmidt numbers can be calculated by:

$$\mathrm{Sc} = \frac{\mu_w}{\rho_w \times D^{\mathrm{kn}}} \tag{19}$$

The concentration polarisation concentration (CPC) is the ratio of the actual concentration gradient to the theoretical concentration gradient, expressed as C_m/C_f. A high CPC implies a notable concentration polarization effect that could decrease the efficiency of the process and result in increased energy consumption [50,51].

In order to evaluate the permeate flux [Eq. (1)], the temperature and concentration at the membrane surface, T_m and C_m are calculated using Eqs. (20) and (21):

$$f_1 = T_f - \frac{B_m\left(\dfrac{\exp\left[\begin{array}{c}\left(-5.80\times10^{3}/T_m\right)+1.39-4.86\times10^{-2}T_m\\ +4.18\times10^{-5}T_m^2+\left(-1.45\times10^{-8}T_m^3\right)\\ +6.55\log\left(T_m\right)\end{array}\right]}{1+0.57257\left(C_m/\left(1000-C_m\right)\right)}\right)\Delta H_v - P_v}{h_w} \tag{20}$$

$$f_2 = C_f \times \exp\frac{B_m\left(\dfrac{\exp\left[\begin{array}{c}\left(-5.80\times10^{3}/T_m\right)+1.39\\ -4.86\times10^{-2}T_m+4.18\times10^{-5}T_m^2\\ +\left(-1.45\times10^{-8}T_m^3\right)+6.55\log\left(T_m\right)\end{array}\right]}{1+0.57257\left(C_m/\left(1000-C_m\right)\right)}\right)-P_v}{k} \tag{21}$$

The complex nonlinear equations described above were solved using a FORTRAN program that implemented the classical Newton–Raphson method with the Jacobian matrix. This approach is highly effective for solving nonlinear systems of equations, as it facilitates faster convergence and greater accuracy. The method involves computing the Jacobian matrix at each iteration, which is then used to update the current estimate of the solution. This process is repeated until the difference between the previous and current estimates falls below a specified threshold. Once the computational process is completed, the temperature and concentration at the membrane module's surface are established using the same method as that for the steam raiser. The permeate flux is then obtained by employing the determined surface temperature and concentration of the membrane (Fig. 2).

2.2. Multi-staging in VMD

Multi-stage VMD (M-VMD) has recently gained attention as means of enhancing the performance of single stage

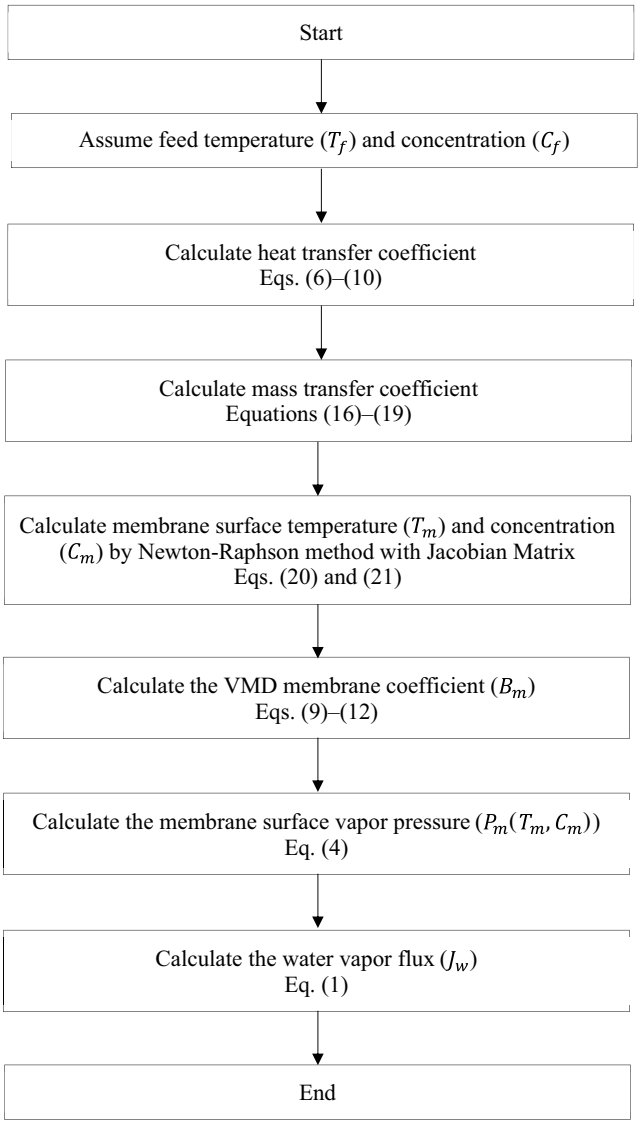

Fig. 2. Procedure (algorithm) used to calculate permeate flux (single-stage VMD).

configuration. In M-VMD process (Fig. 3), the feed solution is heated and then introduced into the first stage of the membrane module. The vacuum on the other side of the membrane causes the liquid to evaporate, while the membrane prevents the liquid from passing through. The resulting vapor is then condensed on a cool surface to form a distillate. The remaining brine solution is then fed into the next stage, where the same process is repeated. The vapor that is produced in each stage is typically recycled and used as the heat source for the next stage, improving the overall efficiency of the process.

If convection heat loss to the environment is negligible, the bulk feed inlet temperature for each stage in succession is obtained using energy balance for the predecessor stage [52]:

$$\Delta H_v = C_{p,w}\left(Q_{b,i}\right)_n\left[\left(T_{b,i}\right)_n - \left(T_{b,o}\right)_n\right] \tag{22}$$

where $(Q_{b,i})_n$ is flow rate of steam from the previous stage.

The above relation can be used to solve for the bulk feed outlet temperature $(T_{b,o})_n$, which will be the bulk feed inlet temperature for the following stage.

The water recovery R_i for a one-stage VMD can be expressed as [36]:

$$R_i = \frac{\eta C_{p,w}\left(T_{b,i} - T_{b,o}\right)}{\Delta H_v} \tag{23}$$

where $(T_{b,i}–T_{b,o})$ is the brine temperature difference between the inlet and outlet of the module and η is the thermal efficiency of the VMD process assumed to be 90% [53].

The water recovery of each stage is given by:

$$R_n = \frac{\left(Q_p\right)_n}{\left(Q_{b,i}\right)_n} = \frac{\left(Q_p\right)_n}{\left(Q_{b,i}\right)_1 \cdot \prod_{i=1}^{n-1}\left(1-R_i\right)} \tag{24}$$

where $(Q_{b,i})_n$ is the brine inlet flux of the module and $(Q_p)_n$ is the permeate flow rate.

The distillate flux at each stage is combined to make a total distillate flux:

$$\left(Q_p\right)_{\text{tot}} = \left(Q_p\right)_1 + \left(Q_p\right)_2 + \cdots + \left(Q_p\right)_n = \sum_{j=1}^{n}\left(Q_p\right)_j \tag{25}$$

By combining Eqs. (24) and (25), the overall water recovery is obtained as:

$$R_{\text{tot}} = \frac{\left(Q_p\right)_{\text{tot}}}{\left(Q_{f,i}\right)_1} = R_1 + \left(1-R_1\right)R_2 + \left(1-R_1\right)\left(1-R_2\right)R_3 + \cdots R_n\prod_{i=1}^{n-1}\left(1-R_i\right) \tag{26}$$

Using the mathematical model developed in this study, the feed outlet temperature, permeate flux and water recovery of the 1st-stage module are calculated. Because the membrane module is successively connected in series, the feed outlet temperature of a previous module is the feed inlet temperature of the next module. The permeate flux $(Q_p)_n$, water recovery R_n and outlet temperature $(T_{b,o})_n$ of the modules can be calculated in turn. Then the total water recovery R_{t0t} is calculated (Fig. 4).

The range of the design and operating parameters used in the numerical simulation are listed in Table 2.

3. Results and discussion

3.1. Model validation

In this study, the accuracy of the developed numerical model was verified by comparing the results obtained from the model with experimental data from previous research conducted on a VMD system for an aqueous NaCl solution at 3 kPa on the permeate side and a 35 g/L feed solution at different flow rates [41]. The results showed a strong agreement between the experimental data and the computational results for feed temperatures ranging from 40°C to 70°C, as illustrated in Fig. 5. A maximum percentage error of less than 5% was observed at various feed temperature settings,

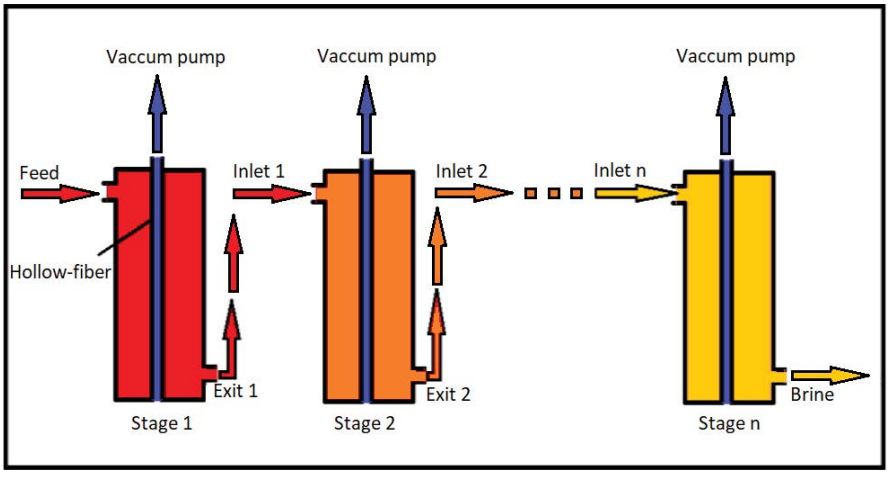

Fig. 3. Schematic representation of M-VMD configuration.

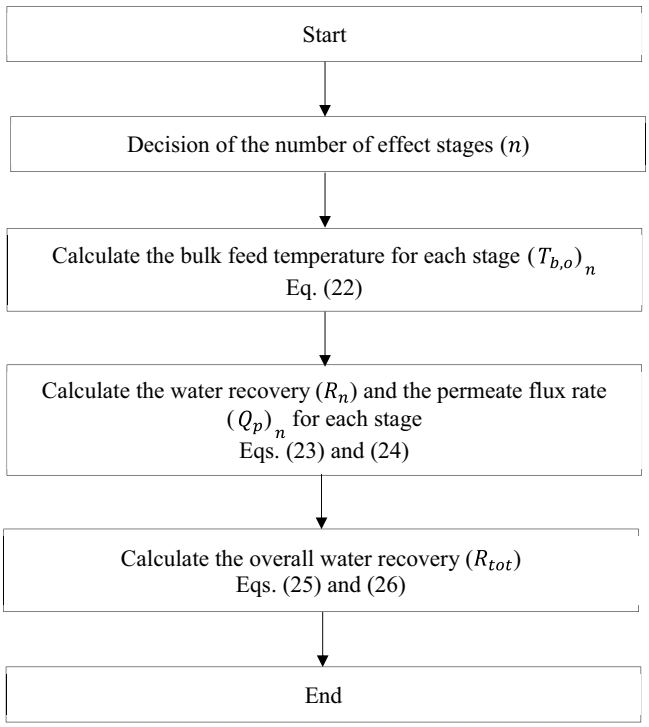

Fig. 4. Procedure (algorithm) used to calculate water recovery (multi-stage VMD).

which is considered acceptable. As a result, the numerical model developed in this study could be used to simulate and design a VMD system for specific operating conditions.

Moreover, the numerical model developed in this study was compared with the mathematical model described by the study of Tang et al. [41] for further validation. The predicted permeate flux for different feed water temperatures at 3 kPa and feed salt concentration of 35 g/L is given in Table 3. It can be seen that the proposed model shows a better agreement with respect to experimental data compared to the previous described model. The mean absolute percentage error (MAPE) values for the present model and the model developed in by the study of Tang et al. [41] are found to be 3.76% and 6.57%, respectively. The high accuracy of the developed numerical model is due to the consideration of both temperature and concentration polarization effects in the model

Table 2
Desing and operating parameters for VMD simulation

Parameter	Value
Feed inlet temperature	40°C–70°C
Vacuum pressure on the permeate side	1–8 kPa
Feed concentration	0–100 g/L
Feed flow rate	30–90 L/h
Number of VMD stages	1–30

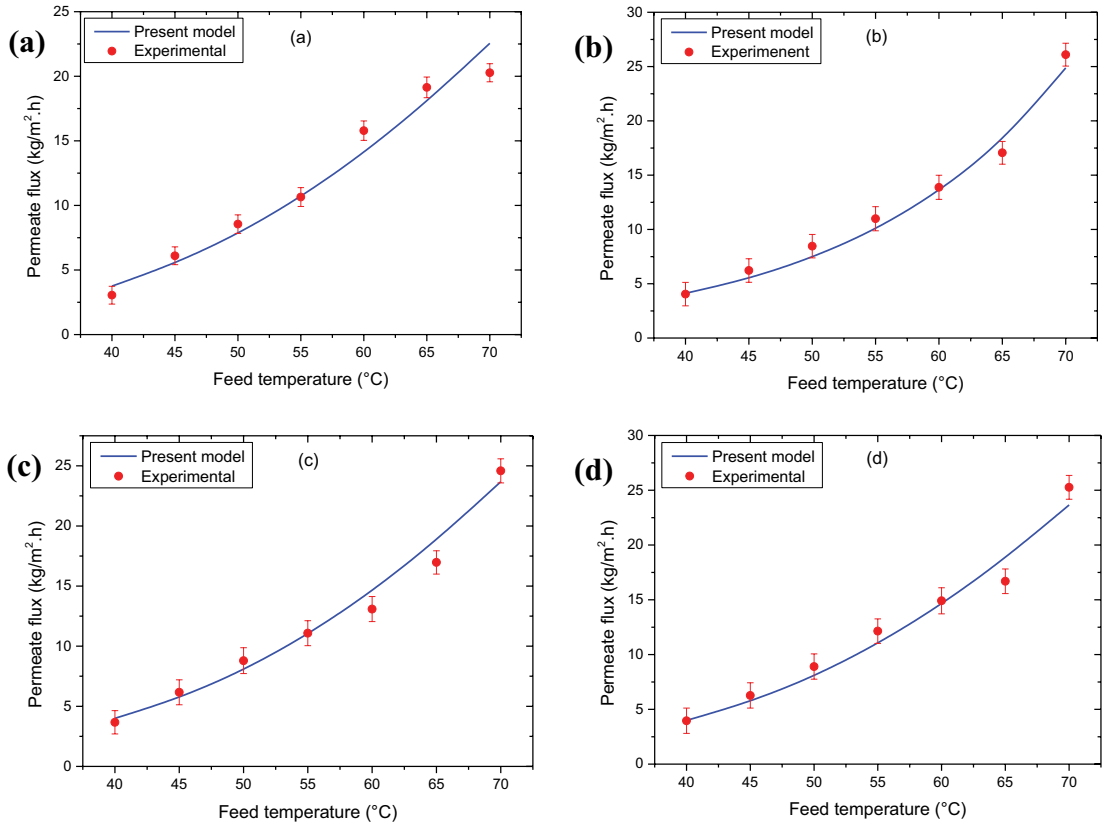

Fig. 5. Comparison of experimental and simulated permeate flux for different feed flow rates (a) feed flux 30 kg/m²·h, (b) feed flux 50 kg/m²·h, (c) feed flux 70 kg/m²·h, and (d) feed flux 80 kg/m²·h.

since heat and mass transfer occur simultaneously in VMD process. In addition, the feed side membrane surface temperature and concentration were computed using numerical solutions. Therefore, all these factors resulted in complicated modeling steps and a more accurate model-based approach.

3.2. Influence of operating parameters

Several operational factors influence the effectiveness of VMD, such as feed temperature, feed flow rate, and water vapor pressure. These parameters influence the feed concentration, permeate flux, as well as membrane characteristics.

3.2.1. Effect of feed temperature

The temperature of the feed solution has a significant impact on the MD process by affecting the partial pressure gradient of water across the membrane. Fig. 6 displays the correlation between feed water temperature and permeate flux. While holding the feed concentration and flow rate at 35 g/L and 50 L/h, respectively, different vacuum pressures were applied, and the feed temperature was varied from 45°C to 70°C. The findings reveal that as the feed temperature rises, the permeate flux increases and follows an exponential pattern at high temperatures. Antoine's equation [Eq. (4)] explains this trend, which connects vapor pressure with feed temperature. For example, for a vacuum pressure of 1 kPa·s, when the feed temperature was raised from 45°C to 50°C, the permeation flux increased by approximately 31%. Similarly, increasing the feed temperature to 55°C, 65°C, and 70°C resulted in permeate flux increases of about 117%, 174%, and 242%, respectively. The driving force for MD is the vapor pressure difference across the membrane module, and elevated feed temperatures produce a greater vapor pressure in the solution, leading to a rise in the permeate flux.

3.2.2. Effect of vacuum pressure

The pressure on the permeate side of the membrane module is a critical factor in the VMD process as it determines the driving force for mass transfer between the pressurized feed side and the vacuum side. As shown in Fig. 7, the permeate flux decreases with an increase in vacuum pressure on the permeate side at various feed temperatures, with a reduction of about 6.2–6.6 kg/m²·h observed when the vacuum pressure is increased from 1 to 8 kPa [Eq. (1)]. This is because the vacuum pressure on the permeate side reduces the pressure difference across the membrane, which is the driving force for the permeation of water vapor through the membrane. As the pressure difference decreases, the driving force for the water vapor to pass through the membrane decreases, leading to a reduction in the permeate flux. Additionally, an increase in vacuum pressure on the permeate side can cause concentration polarization to occur, where the concentration of salt or other dissolved solids near the membrane surface increases due to reduced mass transfer. This can lead to an increase in the resistance to mass transfer, further reducing the permeate flux. However, excessive lowering of the pressure may cause the hydrophobic membrane to become moist, leading to a decrease in salt rejection.

3.2.3. Effect of feed concentration

The concentration of the feed solution is a crucial factor that affects the efficiency of the VMD process. According to Fig. 8, the permeate flux decreases as the salt concentration increases at different flow rates. This decrease is due to the formation of the concentration boundary layer (CBL) parallel to the thermal boundary layer, which decreases vapor transfer resistance and reduces permeate flow [Eq. (15)]. The permeation flux is observed to decrease by about 12%–18% when the salt concentration increases from zero to 40 g/L, owing to the reduced solution vapor pressure caused by dissolved chemicals. Moreover, as the feed concentration increases from zero to 70 and 100 g/L, there is a reduction of approximately 18%–27% and 20%–29% in the permeation flux, respectively. This is because the water activity coefficient decreases, reducing the pushing force across the membrane. The physical properties of the feed water solution, such as increased viscosity and density, affect mass

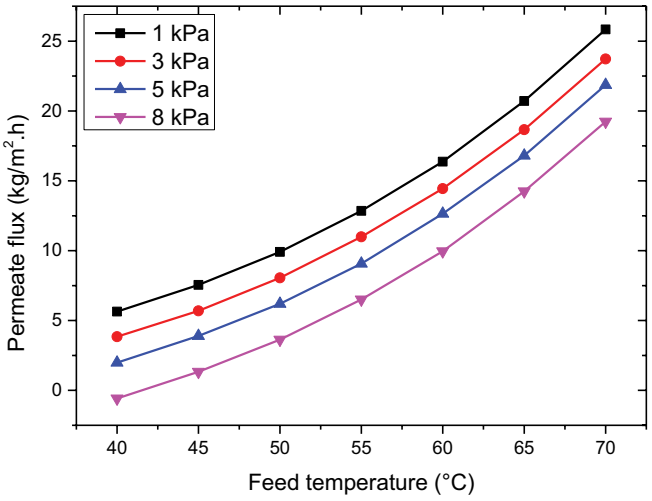

Fig. 6. Effect of feed temperature on permeate flux at different vacuum pressures.

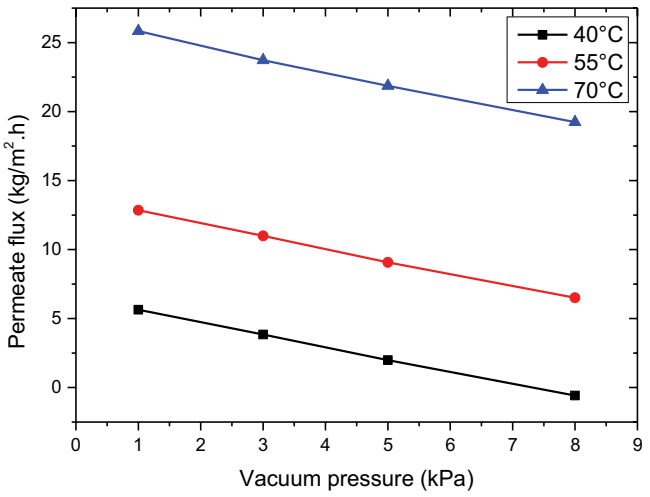

Fig. 7. Effect of vacuum pressure on the permeate flux at different feed temperatures.

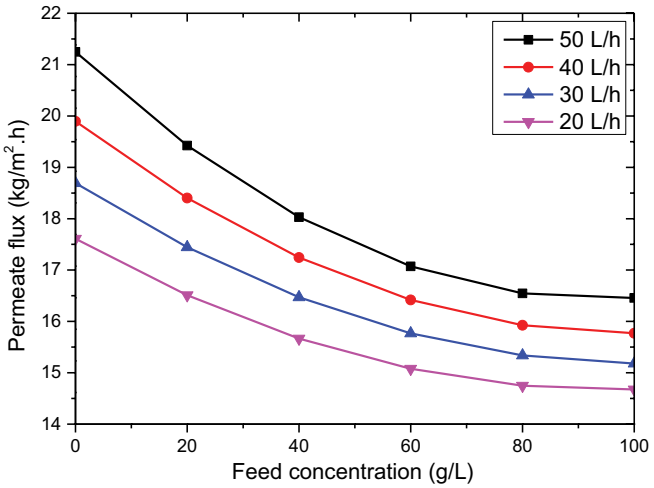

Fig. 8. Effect of concentration on permeation flux at different flow rates.

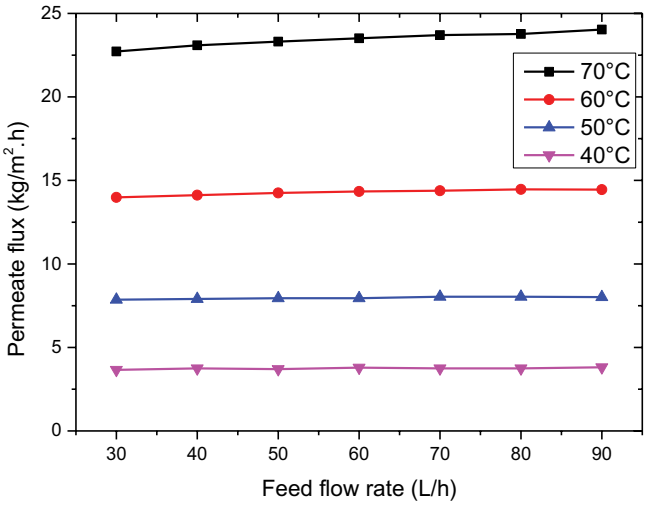

Fig. 9. Effect of feed flow rate on the permeate flux at different feed temperatures.

flow over the membrane by impacting Reynolds number and heat transfer coefficient.

3.2.4. Effect of feed flow rate

The VMD process's efficiency is significantly influenced by the feed flow rate. Fig. 9 shows how the permeate flux changes with variations in feed flow rate and temperature, while the feed solution's concentration is fixed at 35 g/L, and a constant vacuum pressure of 3 kPa is applied to the permeate side. The findings indicate that the permeate flux increases linearly as the feed flow rate rises, and there is no significant effect of the feed temperature on this linear trend of permeate flux concerning the feed flow rate [Eq. (13)]. The thickness of the boundary layer on the feed side decreases as the feed flow rate increases, which enhances the mass transfer coefficient and the permeate flux on the membrane side. Additionally, a decrease in the boundary layer thickness on the hot feed side leads to a reduction in the temperature difference between the feed bulk and the membrane surface, which improves the heat transfer coefficient.

An increase in the feed flow rate from 30 to 40 L/h results in an approximately 1% increase in the permeate flux, while elevating the feed flow rate to 60 and 90 L/h causes an increase in the permeate flux of around 2.5% and 3.3%, respectively. This is due to the more efficient mass transfer and heat transfer coefficient at higher feed flow rates, resulting in higher permeate flux. However, it is important to note that the feed flow rate should be optimized to ensure efficient membrane distillation while avoiding fouling or other operational issues.

3.2.5. Effect of membrane characteristics

The effectiveness of the VMD process is influenced by various membrane characteristics, and the thickness of the membrane is a significant factor affecting the process. Fig. 10 demonstrates how permeate flux is affected by membrane thickness at a constant vacuum pressure of 3 kPa on the permeate side and feed temperatures between

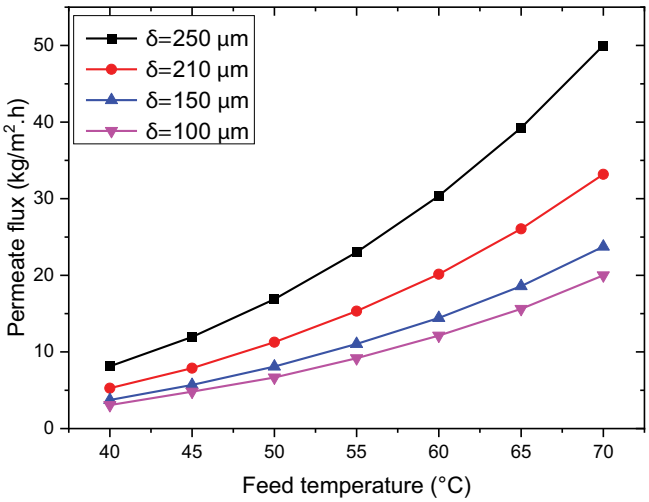

Fig. 10. Effect of membrane thickness on permeation flux.

40°C and 70°C. As membrane thickness decreases, permeate flux increases due to the reduction of mass transfer resistance [Eq. (2)]. However, thinner membranes also result in higher heat loss, creating a trade-off between the benefit of lower heat loss and the disadvantage of lower permeate flux. Fig. 11 displays the influence of membrane porosity on the VMD process. It shows that a higher membrane porosity leads to an increase in permeate flux under similar feed conditions. Membranes with higher porosity offer a larger surface area for evaporation and mass transfer, which reduces mass transfer resistance and enhances mass transfer flux [Eq. (3)]. Improving membrane porosity is especially beneficial for increasing flux at higher temperatures. Moreover, it is important to have a highly porous VMD membrane to prevent wetting.

The membrane material and microstructure have also a significant impact on the performance of VMD. They determine the efficiency of vapor transport across the membrane and, therefore, the overall effectiveness of the process.

Typically, the porous membrane used in MD processes is made of hydrophobic materials such as polypropylene (PP), poly(vinylidene fluoride) (PVDF), and polytetrafluoroethylene (PTFE) in either hollow fiber (HF) or flat-sheet (FS) form. In addition, porous polymeric nanocomposite membrane structure with tuned hydrophobicity has gained much interest. The addition of multi-walled carbon nanotubes (MWCNTs) and silicon dioxide (SiO_2) on the PVDF membrane led to enhanced VMD performance by improving the membrane porosity with finger-like cavities, and thermal and mechanical properties without having significant negative effect on hydrophobicity of the membrane. Synergistic effects of the two additives led to the increase of overall porosity by MWNCTs and growth of macrovoids by SiO_2, even though the effect of MWCNT was more prominent [54].

Nanocomposite PVDF/PTFE membrane was also demonstrated promising performance in the VMD test with the salt rejection of more than 99.9%. The addition of 40% PTFE into the PVDF membrane increased the permeate flux by 464% than the pristine PVDF membrane [55]. Another nanoparticle, such as titanium dioxide (TiO_2), has also remarkably improved the PVDF membrane flux in the VMD test. Compared to the pristine PVDF membrane, more than ten times higher flux was achieved in the test using PVDF membrane loaded with 5 and 2 wt.% of hydrophilic and hydrophobic TiO_2 nanoparticles, respectively [56]. Further optimization of the nanocomposite membrane was conducted by incorporating 7 nm TiO_2, 200 nm TiO_2, and hydrophilic and hydrophobic SiO_2 into the PVDF membrane. Promising results were obtained with the addition of 200 nm TiO_2 nanoparticles at 2% concentration [57]. Carbon-based nanomaterials, such as carbon nanotubes and graphene, have also gained much interest due to their high specific surface area, strength, vapor transport, and tuneable hydrophobicity. Membranes coated by carbon-based nanomaterials exhibit flux enhancement and show anti-fouling properties. Detailed discussion on the carbon-based membrane for MD has been systematically reviewed [58].

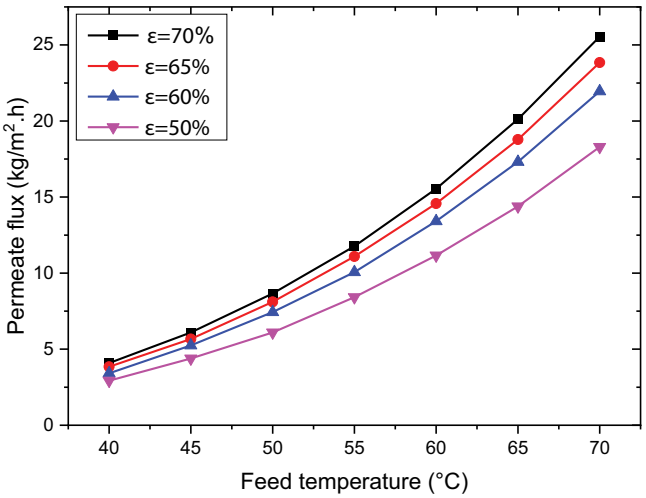

Fig. 11. Effect of membrane porosity on permeation flux.

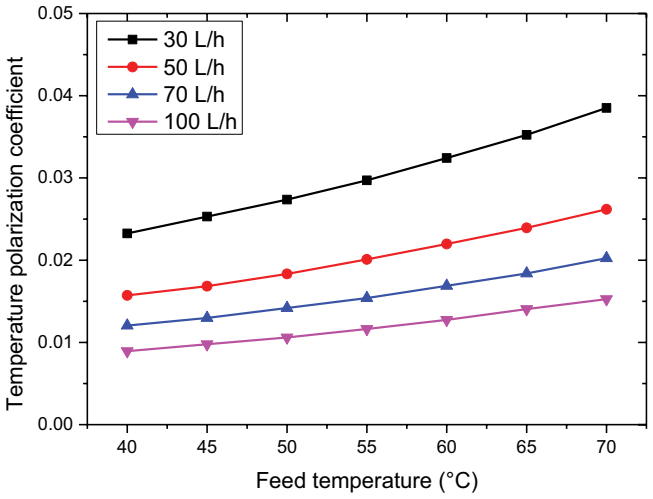

Fig. 12. Effect of feed temperature on temperature polarization.

3.3. Polarization effect

In VMD, polarization effects can occur and impact the performance of the process. Polarization refers to the build-up of temperature gradients and/or concentration gradients at the membrane surface or in the boundary layer adjacent to the membrane. The two main types of polarization effects in VMD are temperature polarization and concentration polarization.

3.3.1. Temperature polarization

The generation of temperature polarization is a significant challenge in MD processes, where a temperature difference exists between the feed bulk and the membrane surface at the liquid/vapor interface. The impact of feed temperature and flow rate on the temperature polarization coefficient is demonstrated in Fig. 12. The simulation was carried out at an absolute pressure of 3 kPa on the vacuum side. The figure indicates that VMD flux increases with an increase in feed temperature, whereas changes in feed flow rate have a minor effect. This rise in VMD flux is attributed to the higher vapor pressure at the top due to increased feed temperature, which enhances the driving force for mass transfer. Moreover, the liquid's reduced viscosity caused by the higher temperature promotes turbulent motion. While increasing the feed flow rate results in a decrease in temperature polarization due to an increase in Reynolds number and heat transfer coefficient, the transmembrane resistance remains the main factor influencing heat and mass transfer, making feed flow rate an insignificant factor in VMD flux.

3.3.2. Concentration polarization

The concentration polarization phenomenon in MD processes arises when the concentration of solutes near the membrane surface becomes higher than that of the bulk feed because of evaporation. Fig. 13 illustrates the effect of feed concentration and temperature on the concentration polarization coefficient (CPC) when the vacuum pressure is 3 kPa, and the feed flow rate is 50 L/h. The CPC values ranging from 1.14 to 1.42 were observed as the feed temperature

increased from 30°C to 40°C. Higher feed concentrations showed a lower concentration polarization effect. This is because an increase in feed concentration leads to a higher concentration of solutes on the membrane surface, reducing the permeate side pressure. Therefore, the concentration gradient decreases, leading to a steady increase in permeation flux. With an increase in feed temperature, the thicker boundary layer due to the increase in permeate flux leads to a higher CPC because more solute is transported towards the membrane and entirely rejected, requiring more solute to diffuse back to the bulk solution. The figure indicates that there was a minor change in CPC values as the feed temperature increased.

3.4. Effect of multi-staging in VMD

Multi-staging in VMD provides the advantages of vacuum distillation and multi-effects to generate high heat and water recovery. Fig. 14a shows the permeate output for each individual stage of a M-VMD process including 30 one-stage modules for different feed water temperatures. The simulation was carried out at 35 g/L feed concentration, 100 L/h feed flow rate and 3 kPa of permeate-side absolute pressure. As can be seen, the water production of each stage decreases gradually along with stage increasing, especially when the feed temperature is high. The reason behind this behavior is that in the initial stages the permeate is higher due to a higher feed solution inlet temperature and a lower salinity as compared to the following stages.

A higher permeate drives out higher energy from the feed side, resulting in a decrease in the feed solution inlet temperature and an increase in the feed concentration for the successive stage. However, the cumulative production increases gradually as shown in Fig. 14a. In addition, the temperature of the first stage is more important to increase

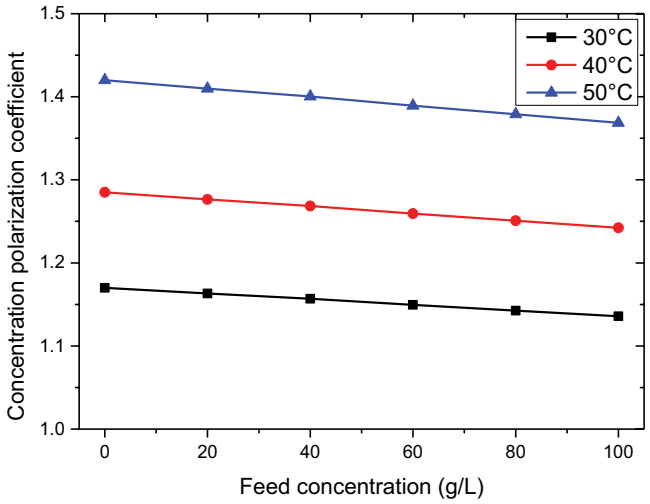

Fig. 13. Effect of feed concentration on concentration polarization.

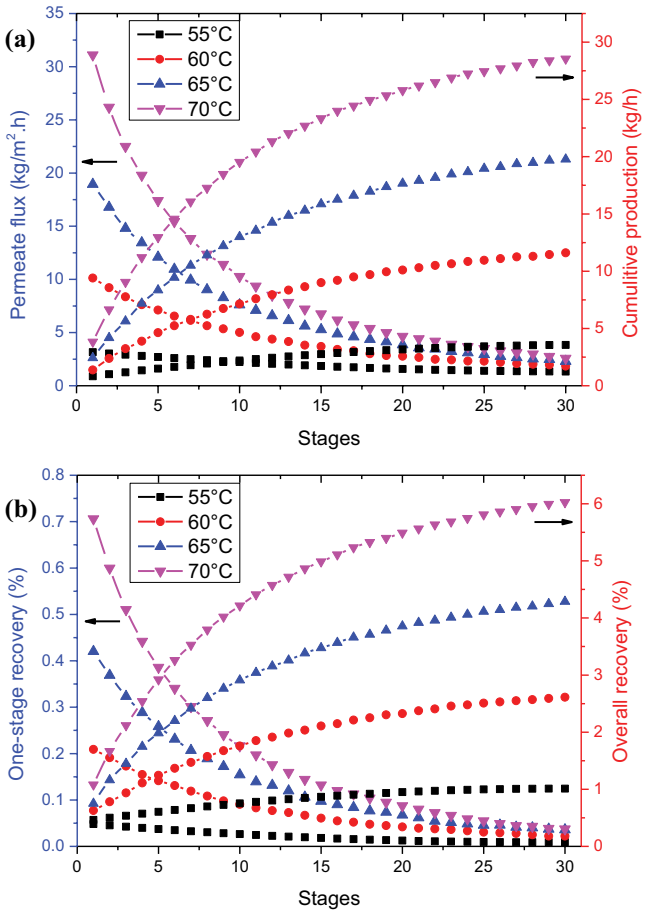

Fig. 14. Effect of muti-staging in vacuum membrane distillation.

Table 3
Prediction models accuracy comparison

Feed temperature (°C)	Permeate flux (kg/m²·h)			MAPE (%)	
	Experimental flux	Present model	Tang et al. [41]	Present model	Tang et al. [41]
40	4.048	4.111	4.112		
45	6.217	5.764	5.550		
50	8.458	8.100	7.492		
55	10.988	10.611	10.113	3.76	6.57
60	13.879	13.543	13.651		
65	17.060	17.901	18.427		
70	26.096	25.449	24.874		

the global water production. The maximum one-stage permeate flux and cumulative production are 31.1 kg/m²·h and 28.5 kg/h when feed temperature is 70°C, respectively. The cross point in Fig. 14a represents the optimum number of stages, giving the maximum possible performance of M-VMD system. The optimum stage number is found to be six when the feed inlet temperature at 1st-stage is 70°C and the permeate-side absolute pressure is 3kPa.

Fig. 14b shows the one-stage and overall water recovery along with stage increasing, which presents the same variation tendency as Fig. 12a. The maximum one-stage and overall recoveries are 0.7% and 6%, respectively, when feed temperature is 70°C. It should be noted that recoveries values cannot exceed more than 7% in a single pass as indicated in literature for DCMD modules [16].

4. Conclusion

In this paper, a comprehensive modeling approach was developed by analyzing heat and mass transfer in both single-stage and multi-stage VMD processes for seawater desalination to evaluate the impact of various operating parameters on the water production and the contribution of polarization to the permeate flux. By identifying critical parameters and understanding the underlying mechanisms governing heat and mass transfer, engineers and researchers can design and operate VMD systems with improved performance and stability. The numerical predictions were compared with previous experimental and numerical results of VMD, and the findings revealed the following:

- The proposed numerical model is providing better fitting with experimental data by introducing polarization concentration phenomenon. As a result, the numerical model developed in this study could be used with confidence to simulate and design a VMD system for specific operating conditions.
- The VMD permeation flux increases with rising feed temperature and flow rate but decreases with increased feed salt concentration and vacuum pressure. At 35 g/L feed concentration, 65°C feed temperature, 50 L/h feed flow rate, and 3 kPa vacuum pressure, the permeation flux reached 18.42 kg/m²·h.
- The VMD process has minimal sensitivity to feed concentration, making it highly advantageous for water desalination.
- The permeate flux increases with membrane porosity and decreases with membrane thickness.
- The most influential factor in determining permeation flux is feed temperature, followed by membrane thickness, vacuum pressure, membrane porosity, feed concentration, and feed flow rate.
- Temperature polarization has a more significant effect on permeate flux than concentration polarization.
- Multi-staging is a promising approach to enhance the performance of VMD, and has the potential to make this process more efficient. However, it is important to optimize the operating conditions for each stage to ensure that the maximum separation efficiency is achieved while minimizing energy consumption.

Finally, it is worth mentioning that fouling has a lesser impact on MD compared to other pressure-driven membrane methods. Nevertheless, it can result in poor performance of the membrane process. Fouling and the accumulation of contaminants on the membrane surface led to reduced effective membrane area and wetting, which causes a decrease in distillate flux and rejection levels. Hence, it is crucial to minimize the effects of these issues to achieve optimum efficiency in the VMD process. This will be published soon as the second part of the current study, using CFD simulations in order to identify areas of high salt concentration and their impact on water vapor flux.

Symbols

A_m	—	Effective membrane area, m²
B_m	—	Permeate coefficient of the membrane, kg/m²/s·Pa
C	—	Solute concentration, g/kg
D^{kn}	—	Diffusion coefficient of solute, m²/s²·s
d_h	—	Hydraulic diameter, m
h_w	—	Heat transfer coefficient, W/m²·s
ΔH_v	—	Latent heat of vaporization, J/kg
J_w	—	Water vapor flux, kg/m²·s
k	—	Mass transfer coefficient, m/s
L	—	Effective length of fiber, m
M	—	Molecular mass of water, kg/mol
P	—	Pressure, Pa
Q	—	Flow rate, L/h
R	—	Gas constant, J/mol·K
	—	Water recovery, %
r	—	Membrane pore radius, m
T	—	Temperature, K

Greek symbols

δ	—	Membrane thickness, m
ε	—	Membrane porosity, –
η	—	Membrane thermal efficiency, %
τ	—	Membrane pore tortuosity, –
P	—	Water density, kg/m
λ	—	Thermal conductivity of the water, W/m·K
μ	—	Dynamic viscosity, Pa/s

Subscripts

b,i	—	Brine, inlet
b,o	—	Brine, outlet
F	—	Feed
i,n	—	Stage number
M	—	Membrane surface
V	—	Vacuum
T	—	Total

Abbreviations

AGMD	—	Air gap membrane distillation
ANN	—	Artificial neural network
CFD	—	Computational fluid dynamics
CBL	—	Concentration boundary layer

CPC	—	Concentration polarization coefficient
DCMD	—	Direct contact membrane distillation
DGM	—	Dusty–Gas model
MD	—	Membrane distillation
M-VMD	—	Multi-stage vacuum membrane distillation
PP	—	Polypropylene
RO	—	Reverse osmosis
SGMD	—	Sweep gaz membrane distillation
TPC	—	Temperature polarization coefficient
VMD	—	Vacuum membrane distillation

References

[1] F. Banat, F.A. Al-Rub, K. Bani-Melhem, Desalination by vacuum membrane distillation: sensitivity analysis, Sep. Purif. Technol., 33 (2003) 75–87.

[2] B. Wu, X. Tan, K. Li, W.K. Teo, Removal of 1,1,1-trichloroethane from water using a poly(vinylidene fluoride) hollow fiber membrane module: vacuum membrane distillation operation, Sep. Purif. Technol., 52 (2006) 301–309.

[3] R. Bagger-Jorgensen, A.S. Meyer, C. Varming, G. Jonsson, Recovery of volatile aroma compounds from black currant juice by vacuum membrane distillation, J. Food Eng., 64 (2004) 23–31.

[4] J.P. Mericq, S. Laborie, C. Cabassud, Vacuum membrane distillation of seawater reverse osmosis brines, Water Res., 44 (2010) 5260–5273.

[5] C. Cabassud, D. Wirth, Membrane distillation for water desalination: how to choose an appropriate membrane?, Desalination, 157 (2003) 307–314.

[6] J. Koo, J. Han, J. Sohn, S. Lee, T.M. Hwang, Experimental comparison of direct contact membrane distillation (DCMD) with vacuum membrane distillation (VMD), Desal. Water Treat., 51 (2013) 6299–6309.

[7] F. Shao, C. Hao, L. Ni, Y. Zhang, R. Du, J. Meng, Z. Liu, C. Xiao, Experimental and theoretical research on N-methyl-2-pyrrolidone concentration by vacuum membrane distillation using polypropylene hollow fiber membrane, J. Membr. Sci., 452 (2014) 157–164.

[8] B.B. Ashoor, S. Mansour, A. Giwa, V. Dufour, S.W. Hasan, Principles and applications of direct contact membrane distillation (DCMD): a comprehensive review, Desalination, 398 (2016) 222–246.

[9] J. Liu, M. Liu, H. Guo, W. Zhang, K. Xu, B. Li, Mass transfer in hollow fiber vacuum membrane distillation process based on membrane structure, J. Membr. Sci., 532 (2017) 115–123.

[10] Z. Liu, Q. Gao, X. Lu, Z. Ma, H. Zhang, C. Wu, Experimental study of the optimal vacuum pressure in vacuum assisted air gap membrane distillation process, Desalination, 414 (2017) 63–72.

[11] L.M. Camacho, L. Dumée, J. Zhang, J.-d. Li, M. Duke, J. Gomez, S. Gray, Advances in membrane distillation for water desalination and purification applications, Water, 5 (2013) 94–196.

[12] A.E. Khalifa, Water and air gap membrane distillation for water desalination – an experimental comparative study, Sep. Purif. Technol., 141 (2015) 276–284.

[13] R.D. Gustafson, J.R. Murphy, A. Achilli, A stepwise model of direct contact membrane distillation for application to large-scale systems: experimental results and model predictions, Desalination 378 (2016) 14–27.

[14] A. Luo, N. Lior, Critical review of membrane distillation performance criteria, Desal. Water Treat., 57 (2016) 20093–20140.

[15] S.O. Olatunji, L.M. Camacho, Heat and mass transport in modeling membrane distillation configurations: a review, Front. Energy Res., 6 (2018) 1–18.

[16] B.B. Kanbur, C. Wu, F. Duan, Multi-criteria thermoeconomic and thermodynamic assessments of the desalination-integrated two-phase liquid-immersion data center cooling system, Int. J. Energy Res., 44 (2020) 10453–10470.

[17] P. Termpiyakul, R. Jiraratananon, S. Srisurichan, Heat and mass transfer characteristics of a direct contact membrane distillation process for desalination, Desalination, 177 (2005) 133–141.

[18] H.Y. Wu, M. Tay, R.W. Field, Novel method for the design and assessment of direct contact membrane distillation modules, J. Membr. Sci., 513 (2016) 260–269.

[19] J.P. Mericq, S. Laborie, C. Cabassud, Vacuum membrane distillation for an integrated seawater desalination process, Desal. Water Treat., 9 (2009) 287–296.

[20] E.A. Mason, A.P. Malinauskas, Gas Transport in Porous Media: The Dusty Gas Model, Elsevier Science Ltd., Amsterdam, 1983.

[21] R. Jackson, Transport in Porous Catalysts, Elsevier Science Ltd., Amsterdam, 1977.

[22] V. Soni, J. Abildskov, G. Jonsson, R. Gani, Modelling and analysis of vacuum membrane distillation for the recovery of volatile aroma compounds from black currant juice, J. Membr. Sci., 320 (2008) 442–455.

[23] S. Upadhyaya, K. Singh, S.P. Chaurasia, M. Agarwal, R.K. Dohare, Parametric Sensitivity Analysis of Vacuum Membrane Distillation for Desalination Process, Proceedings of the International Conference on Chemical, Ecology and Environmental Sciences, ICCEES, Pattaya, December 2011.

[24] J.G. Lee, W.S. Kim, Numerical modeling of the vacuum membrane distillation process, Desalination, 331 (2013) 46–55.

[25] L. Wang, H. Wang, B. Li, Y. Wang, S. Wang, Novel design of liquid distributors for VMD performance improvement based on cross-flow membrane module, Desalination, 336 (2014) 80–86.

[26] H. Hayer, O. Bakhtiari, T. Mohammadi, Analysis of heat and mass transfer in vacuum membrane distillation for water desalination using computational fluid dynamics (CFD), Desal. Water Treat., 55 (2015) 39–52.

[27] Y.D. Kim, Y.B. Kim, S.Y. Woo, Detailed modeling and simulation of an out-in configuration vacuum membrane distillation process, Water Res., 132 (2018) 23–33.

[28] J. Liu, Q. Wang, L. Han, B. Li, Simulation of heat and mass transfer with cross-flow hollow fiber vacuum membrane distillation: the influence of fiber arrangement, Chem. Eng. Res. Des., 119 (2017) 12–22.

[29] M. Asghari, S.G. Lovineh, M. Raji, Numerical simulation and theoretical study on effects of operating parameters in Persian Gulf desalination using vacuum membrane distillation, J. Modell. Eng., 16 (2018) 41–49.

[30] E.N. Dragoi, Y. Vasseghian, Modeling of mass transfer in vacuum membrane distillation process for radioactive wastewater treatment using artificial neural networks, Toxins Rev., 40 (2020) 1526–1535.

[31] S. Ibrahim, Q. Alsalhy, How far can membrane characteristic parameters bestow at the vacuum membrane distillation (VMD) performance: modeling and simulation, Sep. Sci. Technol., 57 (2022) 1211–1233.

[32] R. Sarbatly, C. Chiam, Evaluation of geothermal energy in desalination by vacuum membrane distillation, Appl. Energy, 112 (2013) 737–746.

[33] K. Zhao, W. Heinzl, M. Wenzel, S. Büttner, F. Bollen, G. Lange, S. Heinzl, N. Sarda, Experimental study of the memsys vacuum-multi-effect-membrane-distillation (VMEMD) module, Desalination, 323 (2013) 150–160.

[34] J.G. Lee, W.S. Kim, Numerical study on multi-stage vacuum membrane distillation with economic evaluation, Desalination, 339 (2014) 54–67.

[35] E. Sh. Mohamed, P. Boutikos, E. Mathioulakis, V. Belessiotis, Experimental evaluation of the performance and energy efficiency of a vacuum multi-effect membrane distillation system, Desalination, 408 (2017) 70–80.

[36] Y. Zhang, Y. Peng, S. Ji, J. Qi, S. Wang, Numerical modeling and economic evaluation of two multi-effect vacuum membrane distillation (MEVMD) processes, Desalination, 419 (2017) 39–48.

[37] M.A.E.R. Abu-Zeid, Y. Zhang, H. Dong, L. Zhang, H.L. Chen, L. Hou, A comprehensive review of vacuum membrane distillation technique, Desalination, 356 (2015) 1–14.

[38] K.W. Lawson, D.R. Lloyd, Review: membrane distillation, J. Membr. Sci., 124 (1997) 1–25.

[39] R.W. Schofield, A.G. Fane, C.J.D. Fell, Heat and mass transfer in membrane distillation, J. Membr. Sci., 33 (1987) 299–313.
[40] N. Diban, O.C. Voinea, A. Urtiaga, I. Ortiz, Vacuum membrane distillation of the main pear aroma compound: experimental study and mass transfer modeling, J. Membr. Sci., 326 (2009) 64–75.
[41] N. Tang, Y. Peng, Z. Jia, L. Zhang, J. Xiang, L. Yuan, P. Cheng, X.-k. Wang, Vacuum membrane distillation simulation of desalination using polypropylene hydrophobic microporous membrane, J. Appl. Polym. Sci., 132 (2015) 41632, doi: 10.1002/app.41632.
[42] M.H. Sharqawy, J.H. Lienhard, V.S.M. Zubair, Thermophysical properties of seawater: a review of existing correlation and data, Desal. Water Treat., 16 (2010) 354–380.
[43] S. Bandini, C. Gostoli, G.C. Sarti, Separation efficiency in vacuum membrane distillation, J. Membr. Sci., 73 (1992) 217–229.
[44] L.C. Thomas, Heat Transfer, 2nd ed., Prentice Hall, Englewood Cliffs, NJ, 1992.
[45] F. Laganà, G. Barbieri, E. Drioli, Direct contact membrane distillation: modelling and concentration experiments, J. Membr. Sci., 166 (2000) 1–11.
[46] M. Cherayan, Ultrafiltration and Microfiltration Handbook, CRC Press, 1998.
[47] M. Khayet, Membranes and theoretical modeling of membrane distillation: a review, Adv. Colloid Interface Sci., 164 (2011) 56–88.
[48] R. McCutcheon, M. Elimelech, Influence of concentrative and dilutive internal concentration polarization on flux behavior in forward osmosis, J. Membr. Sci., 284 (2006) 237–247.
[19] J.I. Mengual, M. Khayet, M.P. Godino, Heat and mass transfer in vacuum membrane distillation, Int. J. Heat Mass Transfer, 47 (2004) 865–875.
[50] A. Alkhudhiri, N. Darwish, N. Hilal, Membrane distillation: a comprehensive review, Desalination, 287 (2012) 2–18.
[51] C.K. Chiam, R. Sarbatly, Vacuum membrane distillation processes for aqueous solution treatment–a review, Chem. Eng. Process. Process Intensif., 74 (2013) 27–54.
[52] E. Jang, S.-H. Nam, T.-M. Hwang, S. Lee, Y. Choi, Effect of operating parameters on temperature and concentration polarization in vacuum membrane distillation process, Desal. Water Treat., 54 (2015) 871−880.
[53] H. Fan, Y. Peng, Application of PVDF membranes in desalination and comparison of the VMD and DCMD processes, Chem. Eng. Sci., 79 (2012) 94–102.
[54] R. Zhou, D. Rana, T. Matsuura, C.Q. Lan, Effects of multi-walled carbon nanotubes (MWCNTs) and integrated MWCNTs/SiO_2 nano-additives on PVDF polymeric membranes for vacuum membrane distillation, Sep. Purif. Technol., 217 (2019) 154–163.
[55] Z. Li, D. Rana, T. Matsuura, C.Q. Lan, The performance of polyvinylidene fluoride-polytetrafluoroethylene nanocomposite distillation membranes: an experimental and numerical study, Sep. Purif. Technol., 226 (2019) 192–208.
[56] Z. Li, D. Rana, Z. Wang, T. Matsuura, C.Q. Lan, Synergic effects of hydrophilic and hydrophobic nanoparticles on performance of nanocomposite distillation membranes: an experimental and numerical study, Sep. Purif. Technol., 202 (2018) 45–58.
[57] V. Murugesan, D. Rana, T. Matsuura, C.Q. Lan, Optimization of nanocomposite membrane for vacuum membrane distillation (VMD) using static and continuous flow cells: effect of nanoparticles and film thickness, Sep. Purif. Technol., 241 (2020) 116685, doi: 10.1016/j.seppur.2020.116685.
[58] S. Leaper, A. Abdel-Karim, P. Gorgojo, The use of carbon nanomaterials in membrane distillation membranes: a review, Front. Chem. Sci. Eng., 15 (2021) 755–774.